GRADIVA

Volume 65 | Issue 03 | March 2026
DOI: 10.5281/zenodo.19125314

A High Efficiency Wide Bandgap Transistor Based LCL-T DC-DC Converter for Charging EV Batteries of Wide Voltage Range

Valentine S. Enyi[1], Candidus U. Eya[2]* & Marcel U. Agu[3]

1,2,3Department of Electrical Engineering, University of Nigeria, Nsukka, Nigeria.
1,2,3Africa Centre of Excellence for Sustainable power and Energy Development, University of Nigeria, Nsukka, Nigeria.
1Department of Electrical and Electronic Engineering, State University of Medical and Applied Sciences (SUMAS) Igbo-Eno Enugu State, Nigeria.
*Corresponding Author Email: candidus.eya@unn.edu.ng

Abstract

This paper introduces a bidirectional LCL-T power conversion topology that employs wide-bandgap semiconductor switches to achieve improved energy performance in electric vehicle battery charging applications with significant operating voltage variation. The converter operates at a relatively high frequency equal to the LCL-T resonant frequency to ensure reduced circuit magnetic component size, enhance circuit efficiency and obtain improved range of WBG transistor soft switching over the wide range of battery voltage variation. The LCL-T DC-DC converter, controlled at fixed input dc link voltage by an efficient phase angle shift modulation scheme on hand and then by input dc link voltage variation on the other hand, is first described and then analyzed using first harmonic approximation (FHA). The operational characteristics of a representative controlled LCL-T DC–DC converter are analyzed across a battery output voltage span of 150 V to 950 V, following a defined electric vehicle charging profile. For each mode of control (phase shift angle modulation at constant input dc link voltage OR input dc link voltage variation at zero shift phase angle in sympathy with the output battery voltage variation), the LCL-T DC-DC converter shows high efficiency values around 97%, improved range of transistor soft switching and easily controllable bidirectional capability.

Index Terms – *Resonant LCL-T Converter, Fixed Frequency, EV Charging Profile, Phase Angle Shift Control, dc Link Voltage Control, Wide Bandgap Devices, Wide Battery Voltage Variation, Soft Switching, High Efficiency.*

1. INTRODUCTION

Research and development activities to realize improved electric vehicle (EV) battery chargers have been progressively a major contribution to the ongoing global effort to achieve carbon-emission free environment. This work focuses on the development of efficient and cost-effective bidirectional chargers for electric vehicle batteries. Emphasis is placed on compact size, low weight, and reduced charging time to support faster adoption of electric vehicles over fossil-fuel alternatives. Much improved battery technology, high frequency operation and low loss semiconductor devices significantly help in reducing the size of circuit passive components to realize the above-mentioned desirable performance of the EV battery charger [1].

Fig. 1 presents the operational block representation of the isolated bidirectional battery charging system. The configuration includes an input power conditioning stage responsible for establishing the DC-link voltage V_s. This DC-link then supplies an isolated bidirectional resonant DC–DC conversion stage, which regulates the charging current delivered to the electric vehicle battery.

Volume 65 | Issue 03 | March 2026
DOI: 10.5281/zenodo.19125314

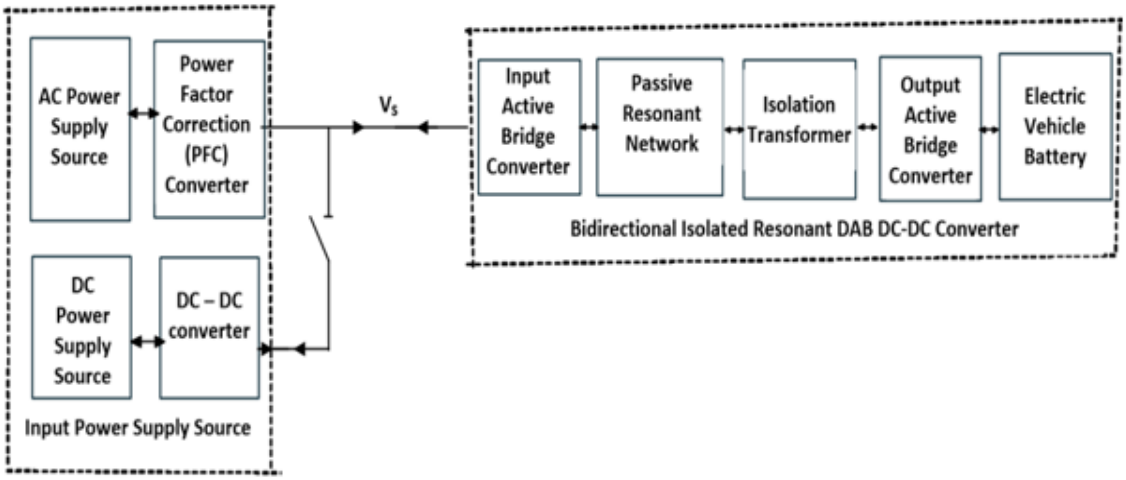

Fig.1: Structural Overview of the isolated Bidirectional Electric Vehicle Battery Charging system

For ac input power source, a bidirectional power factor correction (PFC) ac to dc converter is introduced as shown to make the ac source supply the dc link voltage V_s at unity power factor. When the system is supplied from a DC source such as a DC grid or renewable energy units including photovoltaic arrays, wind energy systems, or fuel cells a bidirectional DC–DC conversion stage is employed, as depicted, to regulate the DC-link voltage V_s to the desired operating level.

This paper examines the isolated bidirectional DC–DC stage in Fig. 1, which is powered by the DC-link voltage V_s. The converter adopts a dual active bridge configuration, coupling the input and output bridges via an isolation transformer and a resonant passive network, with the EV battery connected at the output.

Among the various bidirectional galvanically isolated DC power conversion architectures investigated as reported in prior studies, resonant DC–DC converters [2], [3], [4], [5], [6] are generally preferred to conventional dual active bridge (DAB) converters [7], [8], [9], [10] that rely solely on link inductance for charging current shaping. Additionally, among bidirectional resonant DC–DC converters studied in the literature, the CLLC-based topology exhibits superior performance, delivering improved energy performance and compact design over a broad operating range for electric vehicles battery voltages [11][12]. This is maintained under either pulse frequency modulation (PFM) control at a fixed DC bus voltage variation control at a fixed operating frequency [13], [14], [15]. In this paper, an improved high efficiency silicon (SIC) transistor switched bidirectional resonant LCL-T DC–DC power conversion stage for charging EV batteries of wide battery voltage range of 150V – 950V is proposed. The LCL-T DC–DC converter investigated in this work is regulated at a fixed operating frequency corresponding to the natural oscillation frequency of the LCL-T tank. Using this control method, the output of the input bridge and the input of the output bridge are controlled to follow AC waveform profiles, which removes the necessity for DC-blocking capacitors in the system. Compared with earlier resonant LCL-T designs [16], this approach effectively doubles the battery charging power for a given set of circuit parameters while maintaining elevated efficiency over a broad operating range of electric vehicle battery voltages. Such regulation ensures precise current shaping and supports bidirectional operation,

Volume 65 | Issue 03 | March 2026
DOI: 10.5281/zenodo.19125314

making the converter highly suitable for EV applications requiring rapid and efficient charging. This new proposed resonant LCL-T DC-DC converter performance is hereby described and analyzed to show its merits over the presently highly rated and commonly used resonant CLLC DC–DC power conversion stage for electric vehicle battery charging.

2. PROPOSED HIGH-PERFORMANCE BIDIRECTIONAL DC–DC CONVERTER FOR EV BATTERY CHARGING USING WIDE-BANDGAP (WBG) SWITCHES

The comprehensive circuit diagram of the proposed "wide bandgap (WBG) semiconductor switch-based DC-DC bidirectional converter for high efficiency charging of electric vehicle EV batteries of different voltage levels" is presented in Fig. 2.

For ac input power source, a bidirectional power factor correction (PFC) ac to dc converter is introduced as shown to make the ac source supply the dc link voltage V_s at unity power factor. When the system is supplied from a DC source such as a DC grid or renewable energy units including photovoltaic arrays, wind energy systems, or fuel cells a bidirectional DC–DC conversion stage is employed, as depicted, to regulate the DC-link voltage V_s to the desired operating level.

This paper examines the isolated bidirectional DC–DC stage in Fig. 1, which is powered by the DC-link voltage V_s. The converter adopts a dual active bridge configuration, coupling the input and output bridges via an isolation transformer and a resonant passive network, with the EV battery connected at the output.

Among the various bidirectional galvanically isolated DC power conversion architectures investigated as reported in prior studies, resonant DC–DC converters [2], [3], [4], [5], [6] are generally preferred to conventional dual active bridge (DAB) converters [7], [8], [9], [10] that rely solely on link inductance for charging current shaping. Additionally, among bidirectional resonant DC–DC converters studied in the literature, the CLLC-based topology exhibits superior performance, delivering improved energy performance and compact design over a broad operating range for electric vehicles battery voltages [11][12]. This is maintained under either pulse frequency modulation (PFM) control at a fixed DC bus voltage variation control at a fixed operating frequency [13], [14], [15]. In this paper, an improved high efficiency silicon (SIC) transistor switched bidirectional resonant LCL-T DC–DC power conversion stage for charging EV batteries of wide battery voltage range of 150V – 950V is proposed. The LCL-T DC–DC converter investigated in this work is regulated at a fixed operating frequency corresponding to the natural oscillation frequency of the LCL-T tank. Using this control method, the output of the input bridge and the input of the output bridge are controlled to follow AC waveform profiles, which removes the necessity for DC-blocking capacitors in the system. Compared with earlier resonant LCL-T designs [16], this approach effectively doubles the battery charging power for a given set of circuit parameters while maintaining elevated efficiency over a broad operating range of electric vehicle battery voltages. Such regulation ensures precise current shaping and supports bidirectional operation, making the converter highly suitable for EV applications requiring rapid and efficient charging. This new proposed resonant LCL-T DC-DC converter performance is hereby described and analyzed to show its merits over the presently highly rated and commonly used resonant CLLC DC–DC power conversion stage for electric vehicle battery charging.

Volume 65 | Issue 03 | March 2026
DOI: 10.5281/zenodo.19125314

3. PROPOSED HIGH-PERFORMANCE BIDIRECTIONAL DC–DC CONVERTER FOR EV BATTERY CHARGING USING WIDE-BANDGAP (WBG) SWITCHES

The comprehensive circuit diagram of the proposed "wide bandgap (WBG) semiconductor switch-based DC-DC bidirectional converter for high efficiency charging of electric vehicle EV batteries of different voltage levels" is presented in Fig. 2.

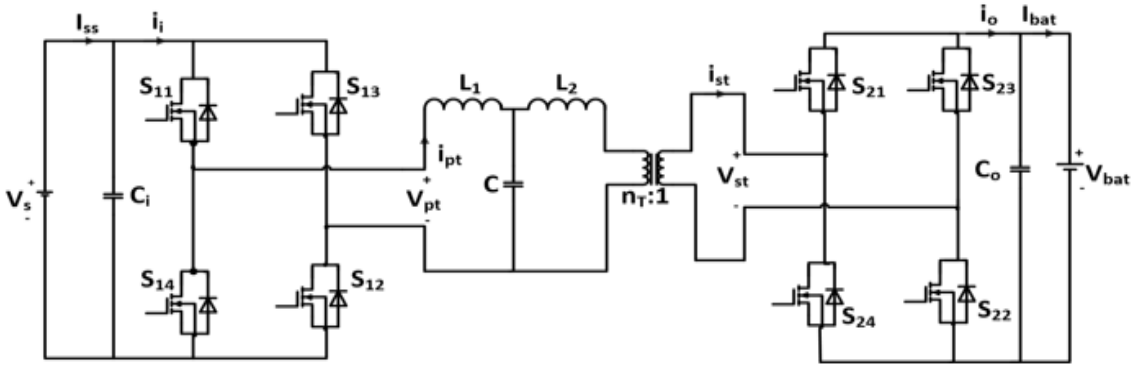

Fig. 2: The Proposed Isolated Bidirectional LCL-T Resonant DC–DC Power Conversion System for Electric Vehicles Battery Charging

The DC bus voltage V_s at the input is connected through a filter capacitor C_i to the input active bridge converter, which employs SiC transistor switches (S_{11}, S_{12}, S_{13} *and* S_{14}). The input active bridge operates at a fixed switching frequency f_s to supply voltage $v_{pt}$to the LCL-T resonant tank (L_1, C, L_2) interconnected with a galvanically isolated transformer with a defined primary-to-secondary winding ratio n_T.

The output active bridge converter, also using SiC switches (S_{21}, S_{22}, S_{23} *and* S_{24}), delivers power to the EV battery, across which the output filter capacitor C_o is connected. For the purpose of the frequency-domain analysis presented, the magnetizing inductance, core resistance, and winding resistances of the isolation transformer are considered negligible, while its equivalent leakage inductance is incorporated into L_2 of the resonant LCL-T tank.

For the resonant LCL-T tank, the inductances are chosen to be equal.

$$L_1 = L_2 = L \tag{1}$$

In the configuration shown in Fig. 2, the DC–DC converter is controlled at a switching frequency f_s that matches the resonant frequency of the LCL-T tank.

$$f_s = f_o = \frac{1}{2\pi\sqrt{LC}}, \quad \text{that is}, \quad \omega_s = \omega_o = \frac{1}{\sqrt{LC}} \tag{2}$$

*w*here ω_s *and* ω_o are respectively the converter switching and LCL-T resonant frequencies in radians/sec.

Also, the magnitude of the reactance of the resonant capacitor C is chosen to be equal to the magnitude of the reactance of each of the resonant inductor L.

$$\omega_s L = \frac{1}{\omega_s C} = X = \sqrt{\frac{L}{C}} \tag{3}$$

Volume 65 | Issue 03 | March 2026
DOI: 10.5281/zenodo.19125314

3.1: Phase-Shift Modulation Control of the Input and the Output Bridge Converter of Fig. 2.

The AC output voltage v_{pt} of the input bridge converter is controlled through a phase-shift modulation technique implemented through the SiC transistor switching sequence illustrated in Fig. 3 where $v_{gs11} - v_{gs14}$ are the 50% duty cycle time variation gating signals to transistors $S_{11} - S_{14}$ and T_s is the switching period ($T_s = \frac{1}{f_s}$).

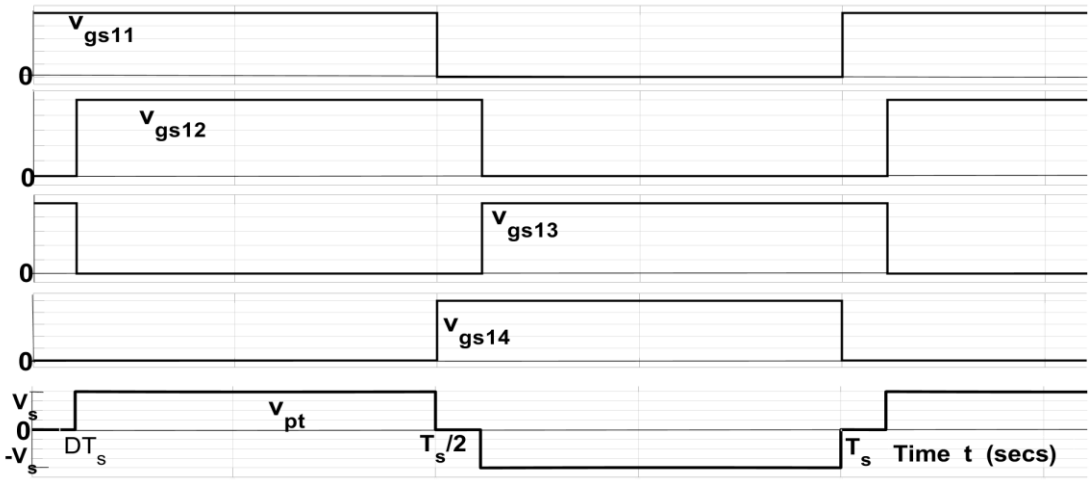

Fig. 3: Time variations of the input bridge converter (Fig. 2) transistor gating signals ($v_{gs11} - v_{gs14}$) and the resultant input bridge converter output voltage v_{pt} for battery charging or forward power flow mode

The control parameter is the time delay DT_s $(0 \leq D \leq 1)$defined as the time interval between the turn-on of switch S_{12} and the turn-on of switch S_{11}. In angular distance, this per cycle lag angle $\emptyset$ of v_{gs12} relative to v_{gs11} is given by

$$\emptyset = \omega_s D T_s = 2\pi D \text{ radians, since } \omega_s T_s = 2\pi \quad (4)$$

From the waveform of v_{pt} (Fig. 3), its rms fundamental component V_{pt1} (in terms of the shift phase angle $\emptyset$ as defined by equation 4) can be shown by Fourier series analysis to be given by:

$$V_{pt1} = \frac{2\sqrt{2}V_s}{\pi} cos\frac{\emptyset}{2} \angle -\frac{\emptyset}{2} \quad (5)$$

Also, the output bridge converter transistors are switched at 50% duty cycle to make its input voltage v_{st} a two-level ac voltage (of amplitude V_{bat}) that lags the reference gating signal by a predetermined angle to be explained later.

3.1.1 The rms Equivalent Circuit of the LCL-T DC-DC Converter of Fig. 2

The LCL-T passive network parameters are usually chosen to present relatively high impedance to harmonic voltage components of v_{pt} and $n_T v_{st}$ higher than their fundamental components. The fundamental RMS AC equivalent circuit of the LCL-T DC–DC converter [17] serves as a representative model for analyzing its AC behavior. This approach focuses on the fundamental frequency components, simplifying the evaluation of voltage and current waveforms while ignoring higher-order harmonics with minimal impact. It facilitates the design of control strategies, tuning of resonant components, and estimation of power losses,

Volume 65 | Issue 03 | March 2026
DOI: 10.5281/zenodo.19125314

providing a practical framework for comparing converter topologies in terms of efficiency, stability, and voltage regulation. Overall, it captures the essential AC dynamics of the system while reducing the complexity of simulations and mathematical analysis. Accordingly, Fig. 4 shows the RMS AC equivalent of the LCL-T DC–DC converter, referenced to the primary side of the high-frequency transformer. The quantities V_{pt1}, I_{pt1} , $\frac{I_{st1}}{n_T}$ and $n_T V_{st1}$ these correspond, respectively, to the RMS fundamental values of the input bridge voltage, input bridge output current, secondary transformer current referenced to the primary, and secondary transformer voltage also referenced to the primary..

From this equivalent circuit, the rms currents (I_{st1} , I_{pt1}) are given by the two voltage loop equations as

$$V_{pt1} - jX * I_{pt1} + jX\left(I_{pt1} - \frac{I_{st1}}{n_T}\right) = 0 \text{ , that is } \quad I_{st1} = -jn_T\frac{V_{pt1}}{X} = n_T\frac{V_{pt1}}{X}\angle -\frac{\pi}{2} \tag{6}$$

$$-jX\left(I_{pt1} - \frac{I_{st1}}{n_T}\right) - jX * \frac{I_{st1}}{n_T} - n_T V_{st1} = 0 \text{ , that is, } I_{pt1} = jn_T\frac{V_{st1}}{X} = n_T\frac{V_{st1}}{X}\angle\frac{\pi}{2} \tag{7}$$

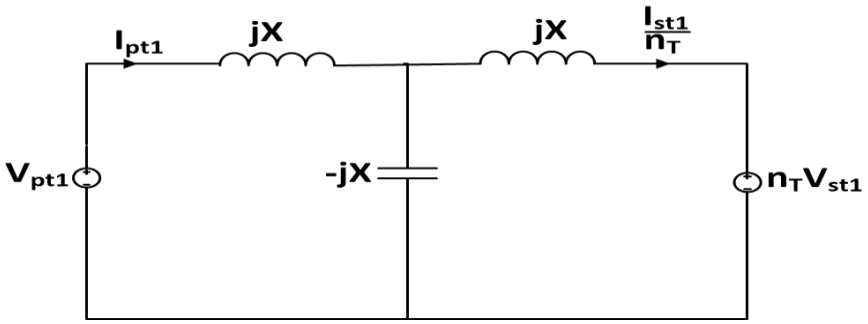

Fig. 4: RMS equivalent model of the LCL-T DC–DC converter depicted in Fig. 2

For synchronous rectification (that is, output bridge converter switches (S_{21} *and* S_{22}) turned on at the instant of zero crossing to positive value of the instantaneous current i_{st}), equation 6 implies that the square wave waveform v_{st} at the output bridge converter input has to be made to lag the fundamental component of v_{pt} by $\frac{\pi}{2}$. Therefore, under synchronous rectification, V_{st1}(which is the fundamental component of v_{st}) is, by Fourier series analysis, given as:

$$V_{st1} = \frac{2\sqrt{2}\,V_{bat}}{\pi}\angle -(\frac{\pi}{2}+\frac{\phi}{2}) \tag{8}$$

Substituting equations 5 and 8 respectively into 6 and 7 gives I_{pt1} *and* I_{st1} under synchronous rectification as

$$I_{pt1} = \frac{2\sqrt{2}n_T V_{bat}}{\pi X}\angle -\frac{\emptyset}{2} \tag{9}$$

$$I_{st1} = \frac{\sqrt{2}n_T Vs}{\pi X}cos(\frac{\emptyset}{2})\angle -(\frac{\pi}{2}+\frac{\emptyset}{2}) \tag{10}$$

Synchronous rectification provides soft switching to many of the converter switches while hard switching for some converter switches is the case.

Volume 65 | Issue 03 | March 2026
DOI: 10.5281/zenodo.19125314

To obtain soft switching [18] for more numbers of the converter transistor switches operating under ZVS or ZCS switching the lagging angle of the output bridge converter input voltage v_{st} is increased to be equal to or very slightly above $\frac{\pi}{2} + \emptyset$. Under this condition, the rms output converter input voltage V_{st1}, the input bridge converter output current I_{pt1} and the output bridge converter input current I_{st1} are respectively adjusted to be

$$V_{st1} = \frac{2\sqrt{2}\,V_{bat}}{\pi} \angle -(\frac{\pi}{2} + \emptyset) \tag{11}$$

$$I_{pt1} = \frac{2\sqrt{2}n_T V_{bat}}{\pi X} \angle -\emptyset \tag{12}$$

$$I_{st1} = \frac{\sqrt{2}n_T V_s}{\pi X} cos(\frac{\emptyset}{2}) \angle -(\frac{\pi}{2} + \frac{\emptyset}{2}) \tag{13}$$

Under active rectification mode of operation six transistor switches turn off under hard switching while all other transistor switching actions are soft switched. Consequently, phase-shift modulation control is implemented using active rectification in this LCL-T resonant DC–DC topology, therefore, active rectification mode of operation is adopted.

To realize active rectification mode of operation during battery charging or forward power flow condition , the gating 50% duty cycle signals v_{gs21} and v_{g22} of the output bridge converter, as easily derived from equation 11, lag the reference gating signal v_{gs11} of the input bridge converter by $\left(\frac{\pi}{2} + \emptyset\right)$ radians. Alternatively

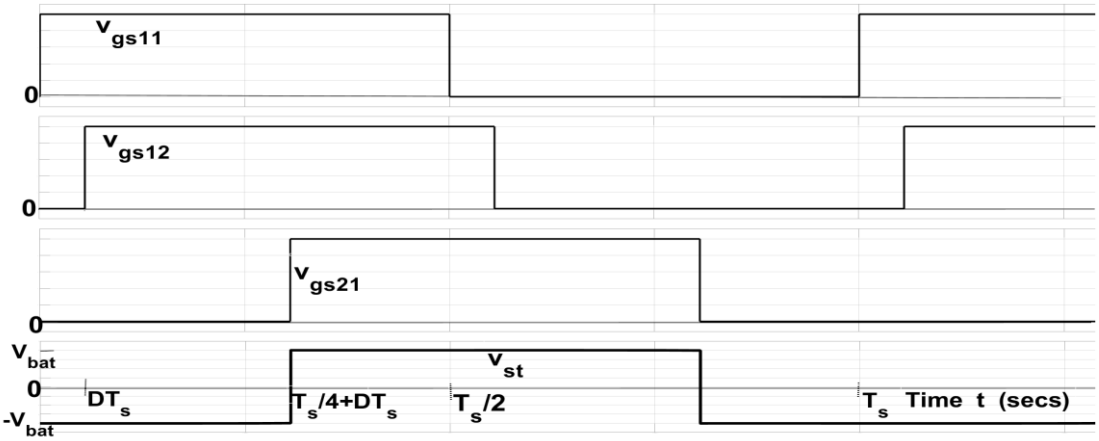

Fig. 5: Time varying waveforms of $v_{gs11}, v_{gs12}, v_{gs21}$ and v_{st} under battery charging (forward power flow) active rectification operation mode

The gating signals v_{gs21} and v_{g22} of the output bridge converter are delayed by $(\frac{T_s}{4} + DT_s)$ seconds with respect to the reference gating signal v_{gs11} under battery charging active rectification operating mode. The gating signals v_{gs23} and v_{g24} of the output bridge converter are respectively the compliments of v_{gs22} and v_{gs21} . Fig. 5 shows the time varying gating signals and the resultant v_{st} under battery charging active rectification mode of operation.

3.1.3. The LCL-T Based DC-DC Converter Forward and Reverse Power Flow Currents and Developed Output Power Using First Harmonic Analysis (FHA)

In active rectification mode of battery charging or forward power flow operation, the instantaneous input bridge converter fundamental output current i_{pt1} and the output bridge

Volume 65 | Issue 03 | March 2026
DOI: 10.5281/zenodo.19125314

converter fundamental input current i_{st1} can easily be derived from equations (12) and (13) as having the expressions:

$$\mathrm{i_{pt1}} = \frac{4n_T V_{bat}}{\pi X}\sin(\omega_s t - \emptyset) \tag{14}$$

$$\mathrm{i_{st1}} = \frac{4\mathrm{n_T V_s}}{\pi \mathrm{X}}\cos(\frac{\emptyset}{2})\sin(\omega_s \mathrm{t} - \left(\frac{\pi}{2} + \frac{\emptyset}{2}\right)) \tag{15}$$

Fig. 6 shows typical time varying waveforms of the source current i_i, the input bridge converter output voltage and current (v_{pt} *and* i_{pt}), the output bridge converter input voltage and current (v_{st} *and* i_{st}) and the output current i_o of the proposed DC-DC converter of Fig. 2 under battery charging conditions. The primary (first-harmonic) terms of $\mathrm{i_{pt}}$ and $\mathrm{i_{st}}$, as given by (14) and (15), are assumed sufficient for deriving near-accurate expressions of the LCL-T DC–DC converter output power [16].

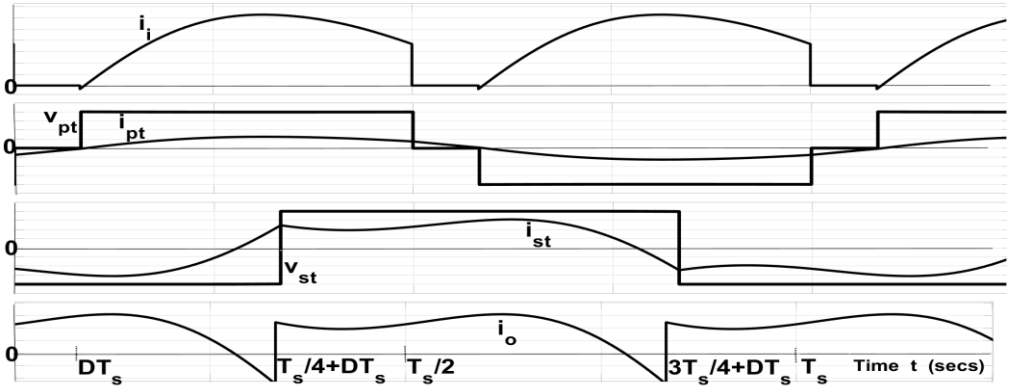

Fig.6: Typical time-domain charging current and voltage profiles obtained from the converter shown in Fig. 2

3.1.3.1 The Power P_O supplied to the battery:

The power P_o supplied to the battery of voltage V_{bat} is

$$P_o = V_{bat} I_o = V_{bat} I_{bat} \tag{16}$$

where $I_o = I_{bat}$ *i*s the average of the output bridge converter output current i_o

One cycle interval of i_o , as shown in Fig. 6, occurs in the time range of $(T_{s/4} + DT_s) - (3T_s/4 + DT_s)$ which is an angular range of $(\frac{\pi}{2} + \emptyset) - \left(\frac{3\pi}{2} + \emptyset\right)$ and in this one cycle interval, $i_o \cong i_{st1}$ as earlier assumed. Therefore, I_o is

$$I_o = \frac{1}{\pi}\int_{\frac{\pi}{2}+\emptyset}^{\frac{3\pi}{2}+\emptyset} i_{st1}\, d\omega t = \frac{1}{\pi}\int_{\frac{\pi}{2}+\emptyset}^{\frac{3\pi}{2}+\emptyset} \frac{4n_T V_s}{\pi X} cos\left(\frac{\emptyset}{2}\right) sin\left(\omega t - \left(\frac{\pi}{2} + \frac{\emptyset}{2}\right)\right) d\omega t = \frac{8n_T V_s}{\pi^2 X} cos^2\left(\frac{\emptyset}{2}\right) \tag{17}$$

Therefore, P_o, from equations 17 and 18 is given by

$$P_o = \frac{8n_T V_s V_{bat}}{\pi^2 X} cos^2\left(\frac{\emptyset}{2}\right), \emptyset \geq 0 \tag{18}$$

Volume 65 | Issue 03 | March 2026
DOI: 10.5281/zenodo.19125314

Equation 18 shows that, for given input voltage V_s, active load (battery) voltage V_{bat}, ratio of transformer windings n_T and the reactance X, the power P_o delivered to the battery is only varied by varying $\emptyset$. This gives one degree of control strategy using the phase shift angle $\emptyset$.

3.1.4. Reverse power flow operation.

Bidirectional power transfer in the reverse direction under active rectification is obtained by assigning negative values to both $\emptyset$ and the term $\left(\frac{\pi}{2}+\emptyset\right)$. This implies making the gating signal v_{gs12} of semiconductor switch S_{12} lead the gating signal v_{gs11} of semiconductor switch $S_{11}$by $\emptyset$ and also making v_{gs21} of semiconductor switch S_{21} to lead the gating signal v_{gs11} of semiconductor switch $S_{11}$by $(\frac{\pi}{2}+\emptyset)$. This gating signal requirement of the input bridge converter of Fig. 2 for reverse power flow is shown in Fig. 7. Fig. 8 shows the typical DC–DC converter circuit waveforms during power flow reversal control.

From Fig. 8, it is evident that the circuit currents are polarity-reversed relative to the forward power flow currents shown in Fig. 6. Therefore, in reverse power flow mode, the output power is the negative of the power expression of equation 18.

$$P_o = -\frac{8n_T V_s V_{bat}}{\pi^2 X} cos^2\left(\frac{\emptyset}{2}\right),\ \&\ \emptyset \leq 0,\ v_{gs21} \text{ leading } v_{gs11} \text{ by phase angle of } (\frac{\pi}{2}+\emptyset) \quad (19)$$

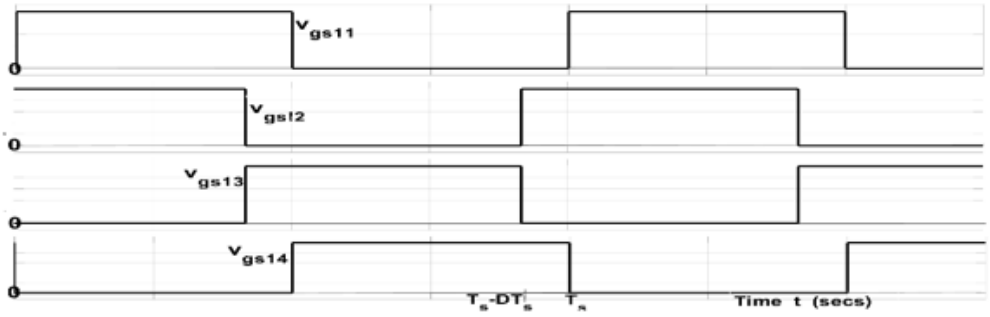

Fig. 7: Time varying waveforms of $v_{gs11}, v_{gs12}, v_{gs13}$ and v_{gs14} under battery discharging or reverse power flow active rectification operation mode

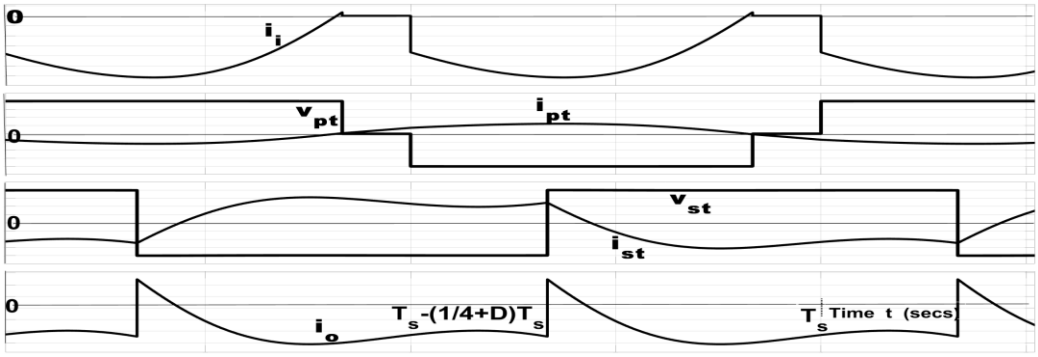

Fig.8: Typical time varying current and voltage waveforms of DC-DC Converter of Fig. 2 under reverse power flow mode

Volume 65 | Issue 03 | March 2026
DOI: 10.5281/zenodo.19125314

Reverse power flow operation exhibits the same range of soft switching as forward power flow operation.

3.2: Control of Bridge Converters in Fig. 2 Based on the Input DC-Link Voltage

In the DC-link voltage variation control of the LCL-T DC–DC converter, the phase-shift angle $\emptyset$ is maintained at zero, while the input DC-link voltage is modulated to regulate the battery charging current according to the prescribed charging profile, accommodating changes in the battery voltage. In this strategy, the bidirectional input stage whether an AC–DC PFC or a DC–DC buck/boost converter, as depicted in Fig. 1 simultaneously manages the DC-link voltage V_s and the battery charging current I_o. Meanwhile, the resonant LCL-T DC–DC stage provides a controlled path for directing the flow of current to the battery, ensuring precise adherence to the charging requirements.

For the analysis of the dc link variation controlled LCL-T DC-DC converter of Fig. 2, additional analysis effort is saved by pointing out that equations 7 to 20 derived above, with $\emptyset$ set to zero, aptly describe the operation of the dc link variation controlled LCL-T DC-DC converter.

3.3. Example Design of the LCL-T topology-based converter

To design a versatile LCL-T bidirectional DC–DC converter capable of charging batteries over a wide voltage range, it is necessary to define the relevant converter specifications, including the battery charging profile.

The battery charging profile depends on the application. In this LCL-T DC-DC converter based EV charger of battery system with wide range of battery voltage variation, the charging profile adopted is constant current (CC) charging over low battery voltage range followed by constant power (CP) charging over high battery voltage range followed finally by constant voltage (CV) charging which maintains the battery voltage constant at its allowed maximum value (V_{batmax})

3.3.1. Specifications of the assumed DC–DC converter employing LCL-T topology

In this design example, Table 1 shows specifications of the assumed DC-DC converter employing LCL-T topology

Table 1: Specifications of the assumed DC–DC converter employing LCL-T topology

Specification item	Value
Range of battery voltage variation ($V_{batmin} - V_{batmax}$)	150V – 950V
Maximum (rated) charging current I_{or}	20 A
Maximum (rated) charging power P_{or}	8Kw
Converter transistor switching frequency f_s	500kHz
Battery charging profile	
Battery Voltage Range of constant current (CC) charging at I_{or} →	150V – 400V
Battery Voltage Range of constant Power charging (CP) at P_{or} →	400V - 950V
Constant Voltage (CV) charging at $V_{bat} = V_{batmax}$ (950V)	

3.3.2. Determination/Selection of Other Converter Circuit Variables/Parameters

(i) The dc input voltage V_s:

In this design, the input DC voltage V_s which corresponds to the fixed DC-link voltage under phase-shift angle control or the maximum DC-link voltage (V_{smax}) in the variable DC-link voltage control method is chosen high enough to reduce current stress on the input bridge

Volume 65 | Issue 03 | March 2026
DOI: 10.5281/zenodo.19125314

of the LCL-T DC–DC conversion stage and to facilitate the operation of the input PFC stage in the EV battery charger. Accordingly, the input DC-link voltage is set to 800 V in this configuration.

(ii) The resonant inductance L:

From equation 18, the inductance L is related to $V_s, I_o, \emptyset, n_T \; and \; f_s$ as

$$I_o = \frac{8n_T V_s}{\pi^2 X} cos^2\left(\frac{\emptyset}{2}\right) = \frac{8n_T V_s}{\pi^2 * 2\pi f_s L} cos^2\left(\frac{\emptyset}{2}\right) \quad (20)$$

For $\emptyset = 0$, the charging current I_o has a maximum value for specified values of $V_s, \emptyset, f_s$ and chosen value of L and this peak current I_o corresponding to the designated maximum charging current I_{or}. Consequently, for voltage equal to 800 V and a transformer turns ratio n_T selected as 2, the resonant inductor value L is determined from the relation:

$$I_{Or} = \frac{\mathbf{8n_T V_s}}{\mathbf{\pi^2 * 2\pi f_s L}}, \text{ that is, } L = \frac{\mathbf{8n_T V_s}}{\mathbf{\pi^2 * 2\pi f_s * I_{or}}} = \frac{\mathbf{8*2*800}}{\mathbf{\pi^2 * 2\pi * 500000 * 20}} = 20.641\mu H \quad (21)$$

(iii) The resonant capacitance C

Since the capacitance C resonates with the inductance L, its value is determined from the equation

$$f_s = f_o = \frac{1}{2\pi\sqrt{LC}}, \text{ i.e }, \; C = \frac{1}{(2\pi f_s)^2 L} = \frac{1}{(2\pi * 500000)^2 * 20.641 * 10^{-6}} = 4.909nF \quad (22)$$

As earlier pointed out, the input and the output bridge converter transistor switches are of the wide bandgap (WBG) silicon carbide (SIC) type to significantly reduce switching losses and make operation at relatively high frequency possible. In this design SIC transistors of 1.2kV are chosen. Also chosen for the design are magnetic components (the inductors and the isolation transformer) made of soft ferrite planar magnetic cores and printed circuit board (PCB) windings for much reduced magnetic losses.

In constant current (CC) charging with I_{or} in the battery variation range of 150V-400V, the battery charging current remains unaffected by variations in the battery voltage for given $V_s, \emptyset, L \; and \; f_s$ as explained using equations 21 and 22. In this example design, the charging current and the phase shift angle in the constant current charging battery voltage varying range of 150V-400V are

$$I_o = I_{bat} = I_{or} = 20 \; A, \;\; \emptyset = 0^o \; , \quad (23a)$$

for the shift phase angle controlled LCL-T converter

$$I_{bat} = I_{or} = 20 \; A, V_s = V_{smax} \; , \quad (23b)$$

for the dc link voltage controlled LCL-T converter

In the constant power (CP) charging range of 400V-950V, the required charging current, $I_o = I_{bat}$, decreases with increase in the battery voltage. Under shift phase angle control, the battery current and the corresponding phase shift angle (from equation 18) are given as:

$$I_o = I_{bat} = \frac{P_{or}}{V_{bat}} \quad (24a)$$

$$\emptyset = 2(cos^{-1}(\sqrt{\frac{\pi^2 * 2\pi f_s L * P_{or}}{8n_T V_s V_{bat}}}) \quad (24b)$$

Volume 65 | Issue 03 | March 2026
DOI: 10.5281/zenodo.19125314

Under dc link voltage variation control equation 24a applies while the associated DC-link voltage V_s is obtained (from equation 19 with $\emptyset = 0$) as:

$$P_{or} = \frac{8n_T V_s V_{bat}}{\pi^2 X}, \text{ that is } V_s = \frac{P_{0r} * \pi^2 * 2\pi f L}{8n_T V_{bat}} \quad (24c)$$

In the constant battery voltage (CV) charging, the charging current is forced to zero ($I_o = 0$) by making $\emptyset = 180^o$ under shift phase angle control or $V_s = 0$ under dc link voltage variation control any instant the battery voltage tries to exceed its allowed maximum voltage $V_{batmax} = 950V$.

Fig. 9 presents the voltage of the battery V_{bat} as a function of the average charging current I_{bat} for the converter based on the LCL-T resonant topology shown in Fig. 2, operating according to the battery charging profile in Table 1 with the specified design parameters.

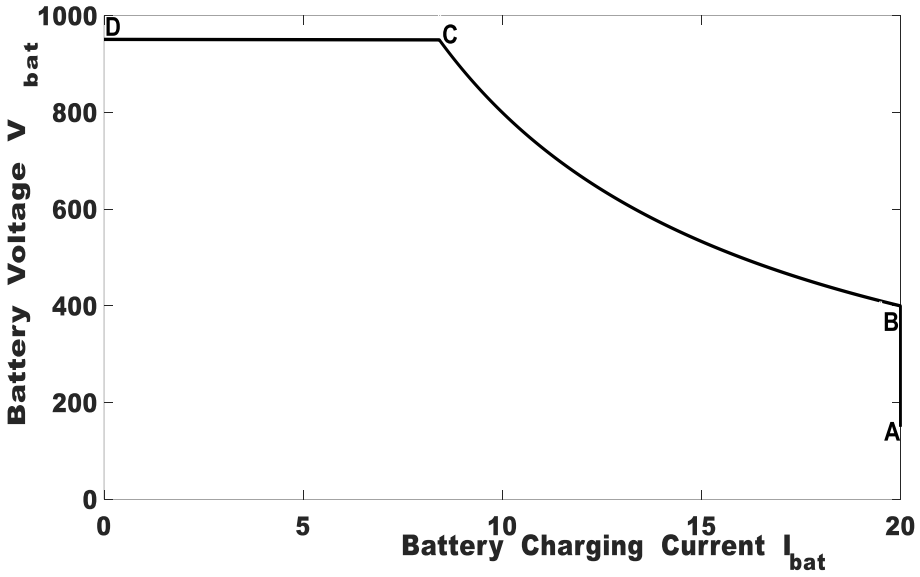

Fig.9: Battery voltage V_{bat} versus charging current I_{bat} (AB→constant current (CC) charging), BC →constant power (CP) charging CD →constant voltage (CV) charging

3.4 Performance Evaluation of the proposed LCL-T DC–DC conversion stage

The LCL-T DC–DC converter described and analyzed in the previous chapter has been modelled and simulated in the MATLAB/Simulink environment. The simulation setup replicates the operational conditions of the converter, including input DC-link variations, bidirectional power flow, and resonant behavior of the LCL-T stage. In the simulation, the converter circuit components are represented together with their specified power loss parameters (such as the SIC transistor on-resistances, the isolating transformer winding resistances, e.t.c).For the entire wide range of converter operation, relevant converter circuit voltage and current time varying waveforms, characteristic performance graphs, range of soft switching and circuit efficiency under both phase shift angle and input dc link voltage variation control schemes are obtained. Relevant comparison and observation are made from these simulated results, the first harmonic analysis (FHA) results and the CLLC DC-DC converter reported in the literature. The converter circuit variables and parameters used in this simulation are those specified in the design example of section 2.2

Volume 65 | Issue 03 | March 2026
DOI: 10.5281/zenodo.19125314

The on resistance r_{Fon} of each of the FET section of the SIC transistor is specified as 50mΩ while the corresponding antiparallel diode on resistance r_{don} is specified to be 10mΩ. The equivalent winding resistance r_{cst} of the isolating transformer referred to the secondary side is specified to be 100mΩ while the intrinsic resistance of each of the converter input and output filter capacitor is specified as 1.0mΩ.

For the LCL-T DC-DC converter operation in accordance with the battery charging profile of Fig. 9, Fig. 10a shows plots of variation of the battery voltage V_{bat} against the shift phase angle ∅ respectively obtained by first harmonic approximation (FHA) and then by MATLAB/Simulink simulation. Not withstanding the very negligible difference between the two plots (especially in the constant current (CC) charging region), the FHA essentially predicts correctly the simulated results. Similarly, Fig. 10b shows sufficiently accurate prediction of the simulated results by first harmonic approximation (FHA) under the dc link voltage variation control of the LCL-T DC-DC converter.

Fig. 11 shows time variation waveforms ($i_i, v_{pt}, i_{pt}, v_{st}, i_{st}$ and i_o) of the LCL-T DC-DC converter of Fig. 2 (with specified design parameters/variables as given above) supplying charging power of 8KW to 600V battery respectively under (a) shift phase angle control and (b) dc link voltage control. From these waveforms (including the observed time-domain voltage and current responses of each SIC transistor of the LCL-T DC-DC converter), it is seen (throughout the entire battery voltage variation range) that the shift phase angle-controlled converter exhibits ten transistor soft switching instants out of the total sixteen transistor switching instants in a cycle of operation.

Conversely, under the same conditions, the DC bus voltage variation-controlled DC–DC converter exhibits eight soft-switching events out of a total of sixteen transistor switching events per operation cycle. Meanwhile, the remaining hard-switched transistors experience negligible instantaneous current at the time of their turn-off.

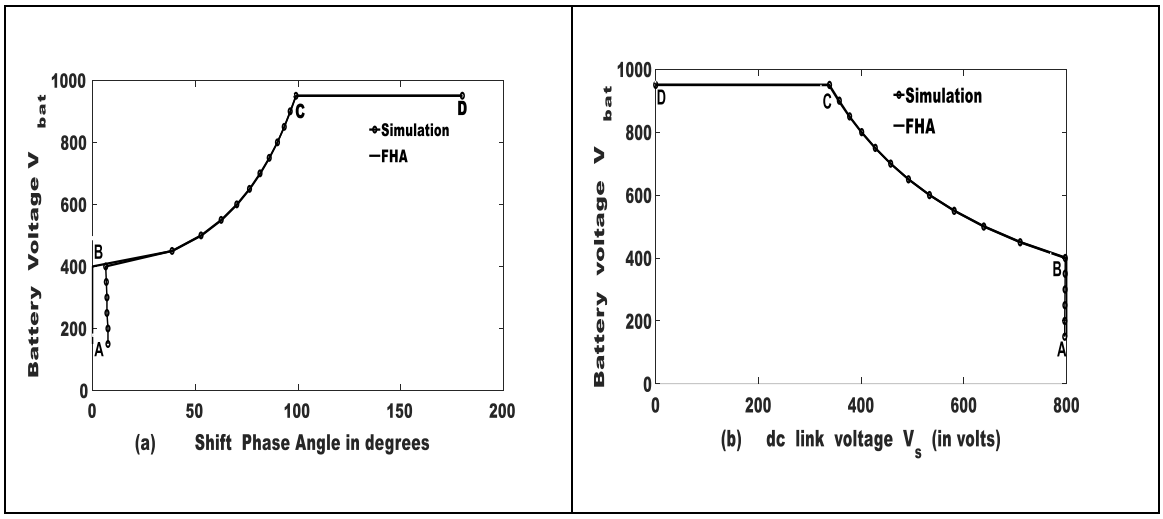

Fig.10: Battery voltage V_{bat} versus (a) phase shift angle ∅ and (b) input dc link voltage V_s (AB→constant current (CC) charging), BC → $constant\ power\ (CP)\ charging$, CD → $constant\ voltage\ charging$)

Volume 65 | Issue 03 | March 2026
DOI: 10.5281/zenodo.19125314

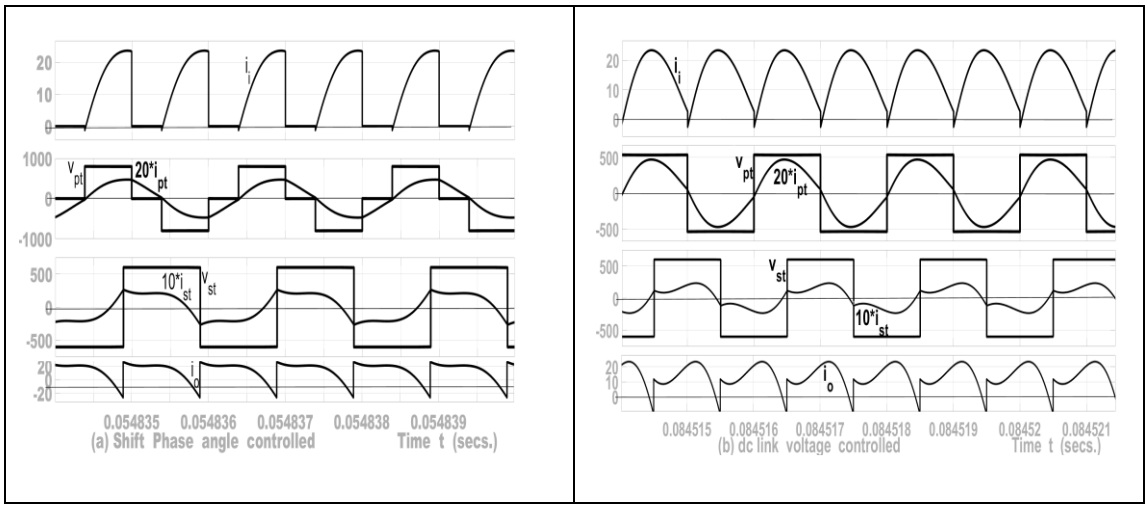

Fig. 11: Time variation waveforms ($i_i, v_{pt}, i_{pt}, v_{st}, i_{st}$ and i_o) of the DC–DC converter with LCL-T configuration depicted in Fig. 2 (with specified design parameters/variables given above) supplying charging power of 8KW to 600V battery ((a) shift phase angle controlled, (b) dc link voltage controlled)

Fig. 12 presents the simulated efficiency curves of the resonant LCL-T-based converter under phase-shift modulation control and under input voltage variation control, following the battery charging profile shown in Fig. 9. Both efficiency plots show that the proposed bidirectional resonant LCL-T DC-DC converter high efficiency is equal to or higher than 97% over the entire wide range of battery voltage variation. This very high efficiency is as high or slightly higher than the best forms of the CLLC and integrated DAB DC-DC converters reported in the literature.

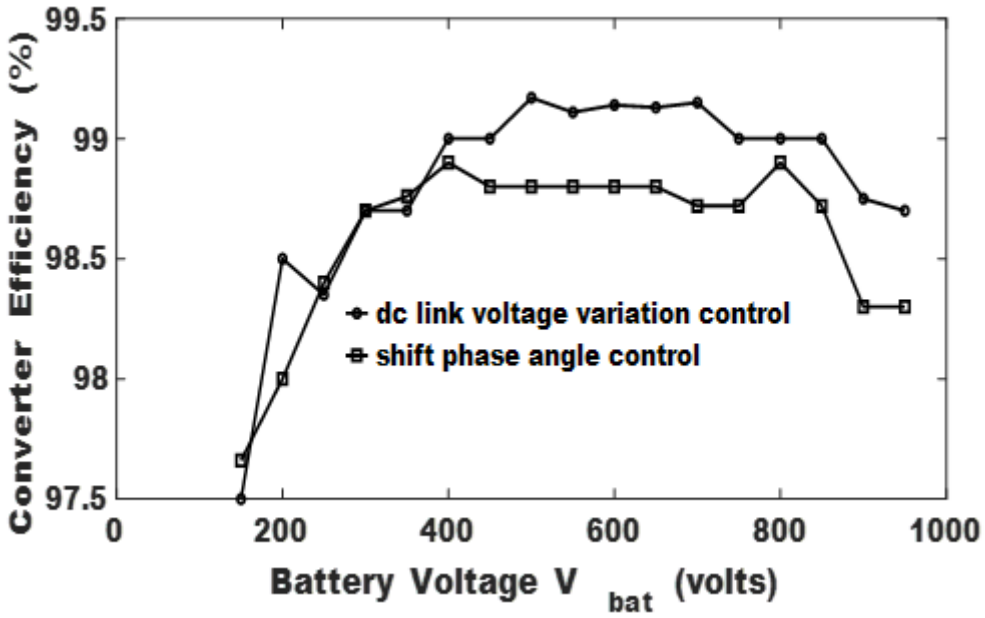

Fig. 12: Efficiency plots of the resonant LCL-T DC–DC converter for phase-shift and input DC bus voltage control modes

Volume 65 | Issue 03 | March 2026
DOI: 10.5281/zenodo.19125314

Other desirable features and performance indices that make the LCL-T DC-DC converter very good for high efficiency charging of EV battery of wide battery voltage variation are outlined as follows:

(i). The DC–DC converter is operated at a constant switching frequency f_s chosen to coincide with the resonant frequency f_o of the LCL-T tank, which improves the overall converter efficiency.

(ii). Between the input bridge converter output and the output bridge converter input, all circuit voltages and currents ($v_{pt}, i_{pt}, v_{st}, i_{st}$) are ac waveforms thus eliminating the usual need of dc blocking capacitors in many reported EV battery chargers and this results in its relative advantage of having reduced circuit components.

(iii). The LCL-T DC-DC constant current to voltage gain ($\frac{I_{st1}}{V_{pt1}} = \frac{I_{pt1}}{V_{st1}} = \frac{n_T}{X}$) is a desirable feature that enhances the DC-DC converter performance across a broad span of battery voltage.

(iv). The LCL-T DC–DC converter has a single control degree of freedom, which can be implemented either through the phase-shift angle ∅ or the input DC bus voltage thus simplifying the circuit control requirements.

(v). The LCL-T DC-DC Converter displays very good bidirectional capability over the entire wide range of battery voltage variation thus making easy the transfer of battery power to the ac/dc input supply grid when the need arises.

4. CONCLUSION

This paper presented an LCL-T configured DC–DC converter capable of bidirectional operation based on wide bandgap (WBG) semiconductor switches for high-efficiency charging of EV batteries across a wide voltage range. The converter was analyzed using the fundamental/first-harmonic approximation (FHA), and a design example covering battery voltages from 150 V to 950 V was provided. Key performance metrics and desirable features, including improved efficiency and lower current stress on the input bridge, and compatibility with varying battery voltages, were highlighted. Compared with previously reported high-performance bidirectional DC–DC converters for EV charging, the proposed LCL-T converter demonstrates competitive advantages in efficiency, control simplicity, and versatility. These attributes support its potential for practical adoption in EV battery charging applications.

References

1) Y. Park, S. Chakraborty and A. Khaligh, “DAB converter for EV on-board chargers using bare-die SIC MOSFETS and leakage integrated planar transformer”, IEEE Trans. Transp. Electrification. Vol. 8, No. 1. pp. 209-224, March 2022.

2) Marcel Ugwuoke Agu, “Principles of Power Electronics Circuits”, 2nd ed. (e-book), University of Nigeria Press, 2023.

3) Zhengmei Lu, Guo Xu, Wenjing Xiong, “A Quasi-Two-Stage Isolated Bidirectional Buck-DAB Converter for Wide Input Voltage Range”, IEEE Transactions on Power Electronics, Vol. 38, No. 2, pp. 1384-1390, February 2023.

Volume 65 | Issue 03 | March 2026
DOI: 10.5281/zenodo.19125314

4) G. Xu, Li. X. Chen, Y. Liu, Y. Sun and M. Su, "Optimized EPS Control to achieve Full Load Range ZVS with Seamless Transition for dual active bridge converters", IEEE Transactions on Industrial Electronics, Vol. 68, No. 9, pp. 8379-8390, September 2021.

5) J. Sun, Q. Sun and P. Wang, "Improved Dynamic Response Strategy with dual phase-shift control for Dual Active Bridge dc-dc Converter", IET Power Electronics, Vol. 13, No. 12, pp. 2671-2674, 2020.

6) H.Shi, H. Wen, J. Chen, Y. Hu. L. Jiang and G. Chen, "Minimum reactive power scheme of dual active bridge DC-DC converter with three level modulated phase-shift control", IEEE Trans. Ind. Appl., Vol. 53, No. 6. pp. 5573-5586, Nov./Dec. 2017.

7) Zhengmei Lu, Mei Su, Guo Xu, Liting Li, Wenjing Xiong and Jianyong Fang, "Switch-Multiplexed Quasi-two-stage Isolated Bidirectional Buck-DAB Converter with full load ZVS Range", IEEE Transactions on Power Electronics, DOI 10.1109/TPEL.2023.3276396.

8) Haoran Li, Shengdong Wang, Zhiliang Zhang, Jingfei Zhang, Wenjie Zhu, Xiaoyong Ren and Cungang Hu, "A Bidirectional Synchronous/Asynchronous Rectifier Control for Wide Battery Voltage Range in SIC Bidirectional LLC Chargers", IEEE Transactions on Power Electronics, Vol. 37, No. 5, pp.6090-6101, May 2022.

9) H. Li *et al*, "Bidirectional Synchronous Rectification on-line calculation control for high voltage applications in SIC Bidirectional LLC Portable Chargers", IEEE Transactions on Power Electronics, Vol. 36, No. 5, pp. 5557-5568, May 2021.

10) Zhengda Zhang, Chunhui Liu, Mengzhi Wang, Yunpeng Si, Yifu Liu and Qin Lei, "High-Efficiency High-Power-Density CLLC Resonant Converter with Low-Stray-Capacitance and Well-Heat-Dissipated Planar Transformer for EV On-Board Charger", IEEE Transactions on Power Electronics, Vol. 35, No. 10, pp. 10831-10851, October 2020.

11) P. He, A. Mallik, A. Sankar and A. Khaligh, "Design of a 1-MHz High-Efficiency High-Power-Density Bidirectional GaN-Based CLLC Converter for Electric Vehicles", IEEE Transactions on Vehicle Technology", Vol. 68, No. 1, pp. 213-223, January 2019.

12) J. H. Jung, H. S. Kim, M. H. Ryu and J. W. Baek, "Design Methodology of Bidirectional CLLC Converter for High Frequency Isolation of dc Distribution Systems", IEEE Transactions on Power Electronics, Vol. 28, No. 4, pp. 1741-1755, April 2013.

13) L. Zhao, Y. Pei, L. Wang, L. Pei, W. Cao and Y. Gan, "Analysis and Design of LCCL Resonant Converter Based on Time Domain Model for Bidirectional On- Board Charger Applications", IEEE Transactions on Power Electronics, Vol. 38, No. 8, pp. 9852-9871, August 2023.

14) Lie Zhao, Yunging Pei, Laili Wang, Long Pei, Zhixiang Li and Wei Cao, "Analysis and Design of LCL Resonant Tank with Reduced Reactive Power for Bidirectional On-Board Charger Applications Utilizing Time-Domain Model", IEEE Transactions on Power Electronics, Vol. 39, No. 4, pp. 4260-4277, April 2024.

15) Z. Guo and M. Li, "An Optimized DPS Control Strategy for LCL Resonant Dual Active Bridge Converter for Wide Voltage Conversion Ratio", IEEE J. Emerg. Sel. Topicsb Ind. Electron, Vol.2, No. 4, pp. 501-512, October 2021.

Volume 65 | Issue 03 | March 2026
DOI: 10.5281/zenodo.19125314

16) Satyaki, Mukherjee, Juan M. Ruiz and Peter Barbosa, “A High-Power Density Wide Range DC-DC Converter for Universal Electric Vehicle Charging”, IEEE Transactions on Power Electronics, Vol. 38, No. 2, pp. 1998-2012, February 2023.

17) Hans Wouters and Wilmar Martinez, “Bidirectional On-Board Chargers for Electric Vehicles: State-of-the-Art and Future Trends”, IEEE Transactions on Power Electronics, Vol. 39, No. 1, pp. 693-716, January 2024.

18) B. Li, F.C. Lee, Q. Li and Z. Liu, “Bidirectional onboard charger architecture and control for achieving ultra-high efficiency with wide battery voltage range”, in Proc. IEEE Appl. Power Electron. Conf. Expo. 2017, pp. 3688-3694.